Proceedings of Shanghai 2017
Global Power and Propulsion Forum
30th October – 1st November, 2017
http://www.gpps.global

GPPS-2017-61

REDUCING LEVELISED COST OF ENERGY AND ENVIRONMENTAL IMPACT OF A HYBRID MICROTURBINE-BASED CONCENTRATED SOLAR POWER PLANT

Davide Iaria
City, University of London
iaria.davide@city.ac.uk
London, UK

Jafar Al Zaili
City, University of London
jafar.alzaili@city.ac.uk
London, UK

Abdulnaser Sayma
City, University of London
a.sayma@city.ac.uk
London, UK

ABSTRACT

A multi-objective optimisation of a hybrid solar dish power plant aiming to minimise the levelised cost of energy while keeping emissions as low as possible is presented in this paper. The analysis was carried out for both regenerative Brayton-Joule regenerative cycle and inter-cooled and re-heated regenerative cycle using an analysis tool developed during this research and validated against available experimental data.

The plant optimisation was performed using a fast and computationally efficient optimisation technique called "response surface optimisation", which generates an approximated function (or response surface) that can be used to find a set of thermodynamic parameters that maximise the plant efficiency while minimising emissions. A Design of Experiment (DOE) Latin hypercube technique was used to generate the training database and a one-dimensional model were used to evaluate the output variables for each point of the database. The DOE was then coupled to a Second Order Polynomial regression technique to approximate the behaviour of the system in the design space. A genetic algorithm was then applied in order to find a high performance arrangement.

Results show a good trade-off between emissions and levelised cost of energy for both plant layouts. The first arrangment shows a minimum levelised cost of energy in the range between 38.5 and 38.8 €cts/kWh with an electrical power production of about 8kW. The second showed a LCOE in the range between 50.5 and 51 €cts/kWh and a net electrical power output of 16 kW.

INTRODUCTION

Parabolic dish systems offer the highest potential solar conversion efficiencies of all the Concentrated Solar Power (CSP) technologies. The concentrator always presents its full aperture directly towards the sun and avoid the efficiency drop due to the "cosine effect", which usually affect other arrangements (Lovegrove, 2012). Parabolic dish CSP can operate as a stand-alone system, eventually generating heat and/or electricity even in areas with no connection to the grid, or can be stacked to form larger power plants in a similar fashion to photovoltaic parks but almost with halved land occupancy. They are, however, the least commercially mature between all CSP plants. These systems have been mainly developed with Stirling engines. Despite their high cycle efficiency, Stirling engines present challenging technological issues resulting in less economic viability.

An alternative to Stirling engines for solar dish applications are micro-gas turbines (MGTs). MGTs are characterised by an open recuperated-Brayton Joule cycle. Intake air is compressed before entering a recuperator where a partial recovery of the exhaust thermal energy allows the net cycle efficiency to approach 30%. Air is then heated in the solar receiver before expansion in the turbine. Nevertheless, MGTs dish concentrated solar power plants are still in the early stage of development and more improvements are required to make them competitive in the market. The OMSoP project (Lanchi et al., 2015) has been investigating the feasibility of coupling a Micro Gas Turbines with CSP Technology for stand-alone solar only operations. However,

the solar resource is not always available and solar fluctuations as well as solar absence during night hours affect plant availability.

Hybrid solar MGTs have the potential to overcome this issue. Hybrid operation, where the solar energy is integrated with a fuel back-up, allows the system to be available during the night and to produce a constant power output during the day despite the high DNI fluctuations. Ragnolo (Ragnolo et al., 2012) compared the performance and the levelised cost of energy of a hybrid solar MGT and hybrid solar Stirling engine for the use in a small-scale solar dish units. The MGT is characterised by a pressure ratio of 3, a turbine inlet temperature (TIT) of 1223 K and a net electrical power output of 25 kW_{el}. According to his study the resulting MGT-dish plant shows a total nominal conversion efficiency and an LCOE around lower than hybrid Stirling engine. Despite recent developments, these systems require further research and some techno-economic issues still need to be addressed. From this point of view, the optimisation of the system is a key aspect to achieve economic competitiveness. In this research, a method to reduce levelised cost of energy and environmental impact of a hybrid solar micro gas turbine operating as a stand-alone system is proposed and discussed.

METHODOLOGY

In order to evaluate the performance of the plant in any working condition, a model for each component of the plant has been developed. As shown by Figure 1, the generic j-th module is mainly characterised by two functions. The first function (or Design Function) calculates the design and the geometrical characteristics of the component, based on the desired set of design variables. The second function (or Off-Design function) evaluates the performances of the plant in off-design condition, based on the design geometrical characteristics calculated by the Design function and the required set of input variables in off-design conditions. The model has been built in C++ language, using object orientated programming.

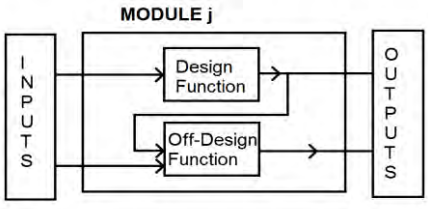

Figure 1. Flow Chart of the generic module

Components models

Compressor

Typically for these applications, the compressor is a centrifugal machine. For these reason, the compressor chosen for this study is centrifugal compressor. The design and off-design performance evaluation have been performed using a one-dimensional model based on the mass, momentum and energy conservation equations. The efficiency of the compressor was evaluated using a set of empirical relationships that can be found in literature (Whitfield and Baines, 1990).

The model has been validated against experimental data for three different compressor sizes (Botha et al. 2005). The validation demonstrates a relative error around 2% in a wide range of operating points for each considered compressor. Figure 2 shows examples of the validation results.

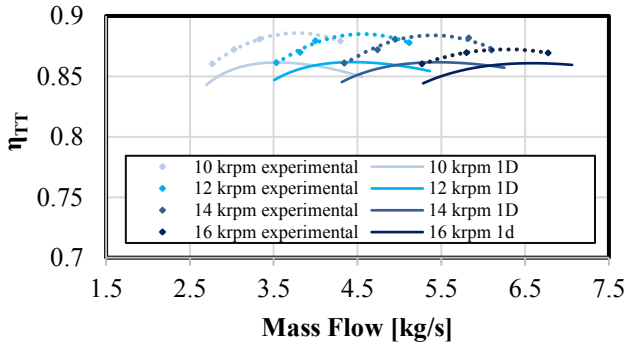

Figure 2. Example of Compressor validation results, efficiency versus mass flow rate for Eckardt Impeller O.

Recuperator & Intercooler

The recuperator chosen for this study is a cross flow plate-fin heat exchanger with off-set strip fins. This arrangement has one of the highest heat transfer to volume ratio between all the heat exchangers available in the market (Ho Sung, 2011). Figure 3 shows a schematic of the heat exchanger and the geometric characteristics of the off-set strip fin.

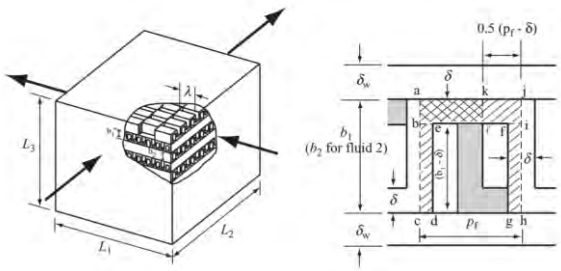

Figure 3. Schematic of a plate-fin heat exchanger, employing off-set strip fin (Ho Sung, 2011).

Design and off-design performances of the heat exchanger have been evaluated using the ε-NTU method. The overall heat transfer coefficient was calculated using eq. 1.

$$UA = \frac{1}{\frac{\delta_W}{k_w A_W} + \frac{1}{\eta_{o1} h_1 A_1} + \frac{1}{\eta_{o2} h_2 A_2}} \quad (1)$$

The convection heat transfer coefficient h was calculated using eq. 2 as a function of the Colburn number J (eq. 3). The Colburn number is a function of the Reynolds number and the geometry. To evaluate this non-dimensional parameter the approach suggested by (Ho Sung, 2011) was applied.

$$h = \frac{JGC_p}{Pr^{2/3}} \quad (2)$$

$$J = f(Re; Geometry) \quad (3)$$

Pressure losses have been evaluated using eq. 4.

$$\Delta p = \frac{1}{2}\rho f v^2 \frac{L}{D_h} \quad (4)$$

In the previous equation v the fluid velocity, L the characteristic length and D_h the hydraulic diameter. The friction factor f was calculated using empirical relationships from the already mentioned approach. The model was validated against available experimental data for a wide range of fin geometries (Yang et al., 2014). Figure 4 shows the friction factor and the Colburn number as a function of the Reynolds number for one of the above mentioned off-set strip fin geometry.

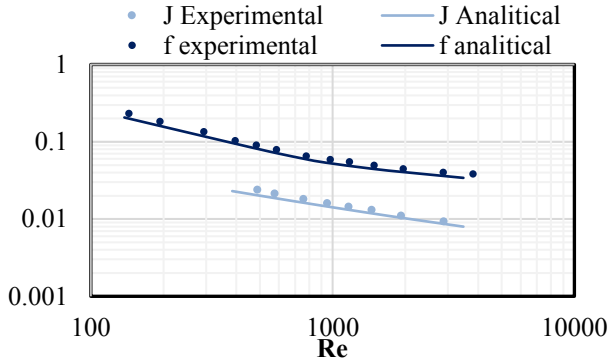

Figure 4. Recuperator validation results for 1/10-27.03 off set strip fin geometry

Receiver & Dish

The Receiver is one of the key component as it significantly affects the plant's performances. The receiver considered in this study is a cylindrical air tube cavity receiver (Qiu et al., 2015). As shown by Figure 5, the receiver is manly composed from a cylindrical cavity surrounded by an insulator. At the bottom of the cavity an optical splitter is present to readdress incident sun rays. At the top of the cavity, a quartz glass is present to minimise heat transfer between the receiver and the ambient.

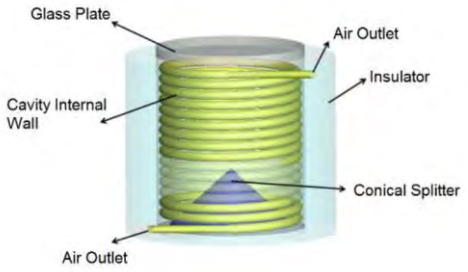

Figure 5. Illustration of the selected receiver in its main components.

As shown by eq. 5 this arrangement is characterised by two main modes of heat losses: convection and radiation losses. These losses were evaluated using empirical relationships available in the literature for a similar design (Zou et al., 2017).

$$Q_{abs} = DNI * A_{dish} * \eta_{dish} - Q_{conv} - Q_{rad} \quad (5)$$

The heat transfer and the pressure losses within the receiver pipes have been evaluated considering empirical relationships for helically coiled tube. The dish optical efficiency was considered constant and equal to 0.8.

Combustion Chamber

The combustor performances have been calculated considering methane as fuel with a higher calorific value of 55 MJ/kg and applying the mass flow and energy equation. Pressure losses were evaluated using the approach suggested by (Lefebvre, 2010).

$$\frac{\Delta p}{p_{in}} = \frac{R}{2}\left(\frac{\Delta p}{q_{ref}}\right)\left(\frac{\dot{m}_{in}T_{in}^{0.5}}{A_{ref}p_{in}}\right)^2 \quad (6)$$

In the previous equation, $\Delta p/q_{ref}$ is the pressure-loss factor and is usually characterised by a value in a range between 20 and 37. For off-design calculations, the combustion efficiency can be calculated as a function of the burner loading coefficient, (Kurzke, 2012) described by eq. 7.

$$\Omega = \frac{\dot{m}}{P_{in}^{1.8} * V_{ref} * e^{\frac{T_{in}}{300\,[K]}}} \quad (7)$$

$$log(1 - \eta_{cc}) = a + b\, log\left(\frac{\Omega}{\Omega_{ds}}\right) \quad (8)$$

$$a = \log(1 - \eta_{cc,ds}) \quad (9)$$

Thus, it is possible to describe the burner part load efficiency, with a single constant, the burner part load constant b, which usually has a value around 1.6.

Turbine

The considered expander is a radial in-flow turbine. Using the same approach adopted for the compressor, the design performance evaluation has been performed using a one-dimensional model based on the mass, momentum and energy conservation equations. The efficiency of the turbine has been evaluated using a set of empirical relationships that can be found in literature (Mustafa et al. 2003).

For off-design calculations, a relationship between pressure ratio, mass flow rate, inlet pressure and temperature is needed. They can be represented in Cartesian coordinate system with the law of the ellipse or Stodola cone. This relationship has been widely applied for steam turbines and is acceptably accurate for a high number of stages, but it is not particularly suitable for radial in-flow turbine application. Moreover, this method doesn't consider the dependency on the rotational speed (Wang et al., 2004).

For the purpose of this study, the formula was modified in order to take into account the dependency on the rotational speed and the turbine polytrophic efficiency.

$$\mu^{off} = \mu * \vartheta * \sqrt{\left[\left(\frac{p_{out}^{off}}{p_{0,i}^{off}}\right)^{\frac{m-1}{m}} - 1\right] / \left[\left(\frac{p_{out}}{p_{0,i}}\right)^{\frac{m-1}{m}} - 1\right]} \quad (10)$$

Where ϑ is a function of the rotational speed, and m is the expansion polytrophic exponent of the thermodynamic transformation.

The model validation was performed by comparing the results in output from the 1D model with experimental results available in literature (Spence, 1997). The validation has been done for a wide range of rotational speeds and pressure ratios for a given turbine design. Figure 6 shows an example of the turbine validation, the charts display the total to static isentropic efficiency of the turbine as a function of the pressure ratio.

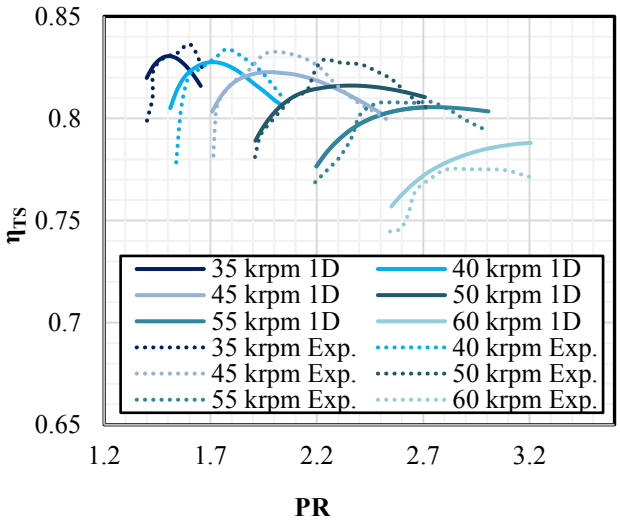

Figure 6. Turbine validation example. Isentropic Total-to-Static efficiency as a function of pressure ratio.

System Layout and Operation strategy

Two different plant arrangement have been considered for this study. The first plant layout is a Brayton-Joule recuperated cycle (Figure 7). For this layout, the operational strategy is to supply fuel in order to ensure that the turbine inlet temperature is kept at the design value during sun hours, regardless of the actual DNI. Then, at a given cut-off DNI, the system is shut down. Rome was selected as location and its solar data of 2009 were used to evaluate the performances of the plant.

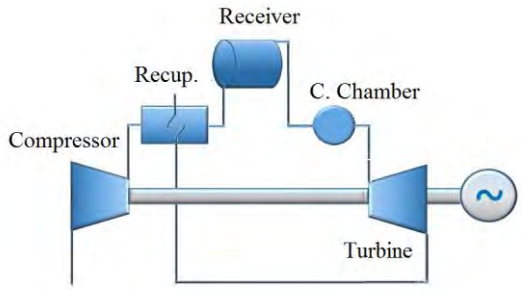

Figure 7. Recuperated Brayton-Joule cycle plant scheme.

The recuperated Brayton-Joule cycle was compared with a second plant layout operating with the same operational strategy. With this purpose, a single shaft intercooled and reheated recuperated cycle was considered. Adopting a single shaft arrangement instead of a dual spool layout can guarantee the applicability of the same operation strategy adopted for the previous case. In both arrangements, the TIT was fixed to be equal to 1073 K. Indeed, a higher temperature could generate significant thermal stresses within the hot parts of the plants, especially for the recuperator and the turbines.

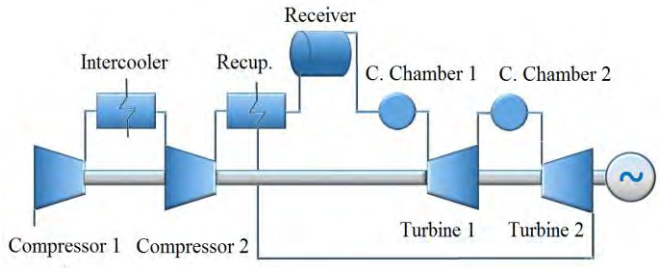

Figure 8. Intercooled and reheated recuperated cycle plant scheme.

Cost Analysis

A detailed techno-economic analysis was carried out to evaluate the cost and the levelised cost of energy of the plant in any arrangement. For this study, the approach used by (Galanti, 2011) has been used and the cost functions for the different components are described by the following equations.

$$C_c = 55.8 * \ln(\mathrm{PR}_c) * \left(\frac{\dot{m}}{0.942 - \eta_{pc}}\right) \quad (11)$$

$$C_t = 376.1 * \ln(\mathrm{PR}_t) * \left(\frac{\dot{m}}{0.903 - \eta_{pt}}\right) \quad (12)$$

$$C_{r/i} = 9 f_m \left(625.1 \dot{m} \left(\frac{p_{in} \Delta p}{100}\right)^{-0.5} * \left(\frac{\varepsilon}{1-\varepsilon}\right)\right) \quad (13)$$

$$C_{cc} = \left(\frac{25.6 * \dot{m}}{0.995 - p_{cc,in}/p_{cc,out}}\right) \quad (14)$$

$$C_{Gen} = 18.7\, P^{0.95} \quad (15)$$

The receiver cost function was extrapolated from a study conducted by (Robertson, 1980) for a similar design.

$$C_{Rec} = 0.0304 * \mathrm{Q_{Rec}} \quad (16)$$

The dish cost was calculated using eq. 18 based on a study conducted by (Gallup, 1994) and updated considering the findings of OMSoP project.

$$C_{Dish} = 260 * \mathrm{A_{dish}} \quad (17)$$

The overall cost can be then calculated using eq. 18.

$$C_{TOT} = C_{MGT} + C_{Receiver} + C_{Dish} + C_{inst} \quad (18)$$

In the previous equation, the installation cost C_{inst}, was estimated as 15% of the total components costs.

Using the Chemical Engineering Plant Cost Index (C.E.P.CI.) each calculated cost was discounted to update prices at the current year (eq. 19).

$$C_{2016} = \frac{C_j * (CEPCI_{2016})}{(CEPCI_j)} \quad (19)$$

The fuel cost was estimated based on the European average price of natural gas in Europe in the second quarter of

2016. According to Eurostat, the European average of methane in the industry sector is 0.032 €/kWh.

The levelised cost of energy can be consequently calculated using eq. 20.

$$LCOE = \frac{\alpha C_{TOT} + C_{fuel} + C_{maint}}{E_{NET}} \quad (20)$$

$$\alpha = \frac{i*(1+i)^n}{(1+i)^n - 1} \quad (21)$$

The discount index α was evaluated considering i=0.7 and n=25 years. Maintenance costs have been estimated to be 5% of the total cost.

Emissions Analysis

The carbon dioxide emissions were evaluated considering the combustion reaction balance normalised in respect of the total energy produced.

$$F_{CO_2} = \frac{44}{12}\frac{m_f}{\chi_{CO_2} E_{NET}} \quad (22)$$

NOx emission were estimated using an empirical relationship available in literature (Kurzke, 2012).

$$F_{NO_x} = 32\left(\frac{p_{in}}{2965000}\right)^{0.4} * e^{\left(\frac{T03off - 826}{194}\right) + 0.118} * \frac{m_f}{10^3 * E_{NET}} \quad (23)$$

Optimisation Technique

The optimisation technique adopted in this paper is called response surface optimisation and generates an approximated function that can be used to find a set of parameters that maximise plant's efficiency. The first step is to select the variables (or parameters) influencing the optimisation process, the input and output parameters. The complexity of the optimisation problem increases exponentially with the number of parameters, for this reason a preliminary sensitivity analysis is required to minimise it and a design of experiment (DOE) technique was applied. The DOE was then followed by a RSM technique to approximate the behaviour of the system in the design space. A multi objective genetic algorithm based on controlled elitism concept was then applied in order to find the optimum solution (Iaria et al., 2016).

RESULTS AND DISCUSSION

Sensitivity analysis

As already mentioned, a preliminary sensitivity analysis is necessary to minimise the number of input parameters and then the computational effort of the optimisation. For this reason, the behaviour of the plant under different combustor inlet temperature, rotational speeds, mass flow rates and pressure ratios was investigated. The sensitivity analysis was carried out considering the recuperated Brayton-Joule cycle.

Figure 9 and Figure 10 show a clear LCOE reduction with increasing combustor inlet temperature and rotational speed. With the variation of these two parameters, the same behaviour has been noticed for CO_2 emissions. On the other hand, further investigations are needed for the variation of the pressure ratio and the mass flow rate. Thus, these two parameters will be the optimisation variables of the problem.

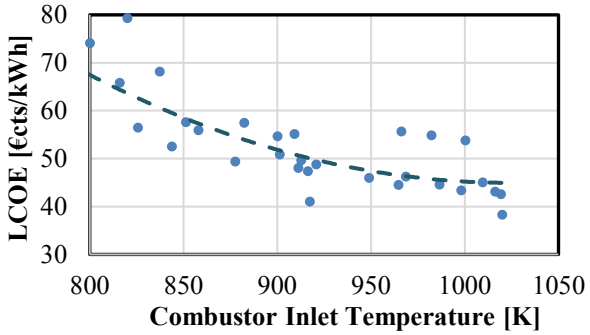

Figure 9. LCOE sensitivity with combustor inlet temperature

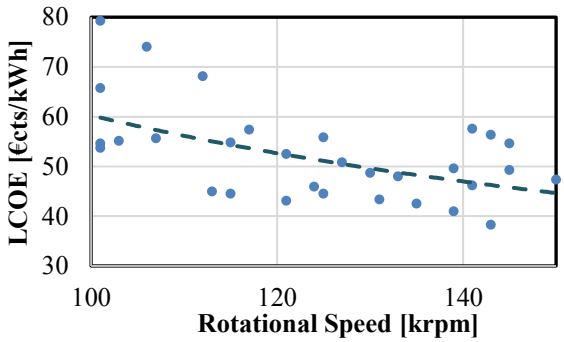

Figure 10. LCOE sensitivity with rotational speed.

Recuperated Brayton-Joule cycle optimisation

Optimisation set-up

The input parameter of this first optimisation are the mass flow rate and the pressure ratio. Their range of variation within the design space is reported in Table 1. This range is based on the results of the sensitivity analysis. The lower bounds were set considering a minimum power requirement of 5 kW. While, the upper bound correspond to high levelised cost of energy.

Table 1. Input parameters range.

	$\dot{m}$	PR
Lower Bound	0.06	2.5
Upper Bound	0.15	4.6

The sensitivity analysis also demonstrates that combustor inlet temperature and rotational speed must be as high as possible. Although, there are some technological aspects to be considered. The combustor inlet temperature was fixed to be equal to 1000 K in design condition to provide the combustor with the minimum required fuel flow rate to guarantee combustion stability in any working conditions. The rotational speed was fixed to be equal to 140 krpm based on a previous study conducted within OMSoP (Lanchi et al., 2015).

Response surface

As already mentioned, the selected regression model is a second-order polynomial response surface. Results show a

good accuracy of the surface with a correlation coefficient between 0.93 and 0.99 and a relative root mean square error below 1% for each output variable (Table 2).

Table 2.Correlation coefficient and relative root mean square error of the surface for each output parameter

	η	P	C_{tot}	LCOE	CO_2	NO_X
R^2	0.96	0.99	0.99	0.96	0.97	0.98
RMSE	0.69	0.95	0.36	0.63	0.61	0.68

Figure 11 shows the response surface of the optimisation. The surface presents a minimum LCOE in the range of pressure ratio between 3 and 3.5 and in the range of mass flow rate between 0.08 and 0.1.

Optimisation results

The optimisation was carried out using a multi objective genetic algorithm based on controlled elitism concept. The objective of the optimisation was to minimise both LCOE and specific CO_2 production. To evaluate the convergence of the optimisation the convergence stability percentage and a maximum allowable Pareto percentage were used. The first represent the stability of the population in the current generation and the typical value of 1% was considered. The second is the ratio between the number of points on the Pareto front and the number of samples in the current generation, in this case the value considered for the convergence was 99%. Figure 12 shows the Pareto front of the optimisation.

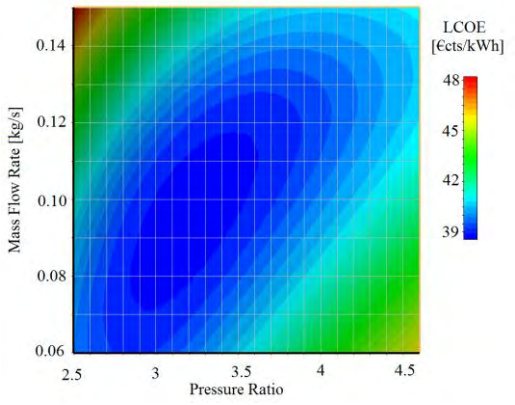

Figure 11. Response surface of the optimisation.

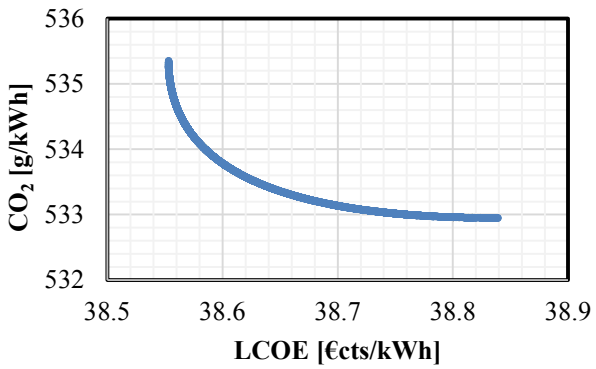

Figure 12. Pareto front of the optimisation.

The optimisation was carried to a certain number of candidate points. One of them was selected and simulated. Table 3 shows the main characteristics of the optimised plant.

Table 3 Performance parameters of the optimised plant.

PR	3.15	**η**	0.238
$\dot{m}$ [kg/s]	0.089	**ηc**	0.78
P[kW]	8.58	**ηr**	0.85
LCOE [€cts/kWh]	38.5	**ηrec**	0.76
CO_2 [g/kWh]	534	**ηcc**	0.97
NO_X [g/kWh]	3.06	**ηt**	0.87
C [€]	22895	**ηdish**	0.8

The results shows a not yet competitive LCOE. Despite this high value of the levelised cost of energy there's still room for improvements. Indeed, as shown in the previous table components performances can be improved, this is especially true for the compressor and the solar receiver. Moreover, Increasing the TIT can be a key feature in increasing the power output. Although, a higher TIT requires more temperature resilient materials and further investigations are needed.

As clearly shown by Figure 13, the most expensive components is the dish. Further technological improvements in its manufacturing processes could be a key feature in reducing the plant capital cost and LCOE.

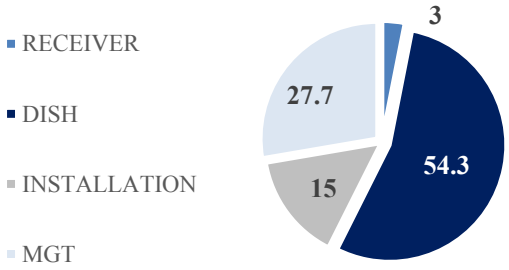

Figure 13. Plant cost breakthrough.

Intercooled and Reheated cycle optimisation

Optimisation set-up

The input parameter of this second optimisation are the mass flow rate and the pressure ratio. Their range of variation within the design space is reported in Table 4. Upper and lower bound have been fixed based on the same criteria mentioned in the previous section.

Table 4. Input parameters range.

	$\dot{m}$	PR
Lower Bound	0.06	2
Upper Bound	0.15	3.5

Response surface

The selected regression model for this second optimisation is a second order polynomial response surface. Results shows a good accuracy of the surface with a

correlation coefficient between 0.93 and 0.99 and a relative root mean square error below 1% for each output variable (Table 5).

Table 5.Correlation coefficient and relative root mean square error of the surface for each output parameter

	η	P	C_{TOT}	LCOE	CO_2	NO_X
R^2	0.95	0.99	0.78	0.92	0.934	0.74
RMSE	1.8	1.7	5.8	1.8	2.0	4.1

Figure 14 shows the response surface of the optimisation. Results demonstrate minimum LCOE in the region of pressure ratio between 2.4 and 2.6 and mass flow rate

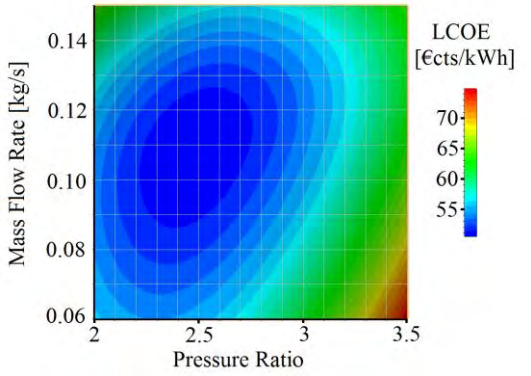

Figure 14. Response surface of the optimisation.

Optimisation results

The optimisation was carried out using the same criteria described previously. Figure 15 shows the Pareto front of the optimisation. The optimisation carried to a certain number of candidate points. One of them was selected and simulated. Table 6 shows the main characteristics of the optimised plant.

Table 6 main characteristics of the optimised plant.

PR	2.452	**ηc1**	0.82
m [kg/s]	0.0985	**ηc2**	0.82
P[kW]	15.2	**ηr**	0.85
LCOE [€cts/kWh]	50.7	**ηi**	0.82
CO_2 [g/kWh]	729	**ηrec**	0.77
NO_X [g/kWh]	6.12	**ηcc**	0.97
C [€]	39430	**ηt1**	0.81
η	0.224	**ηt2**	0.87

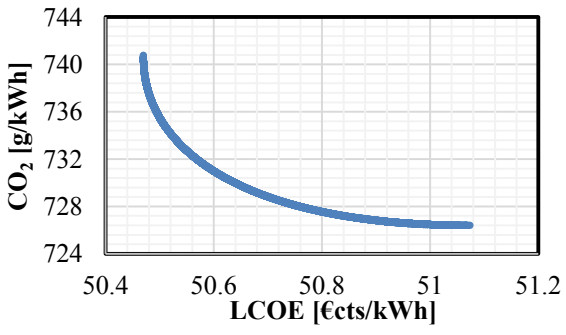

Figure 15. Pareto front of the optimisation.

Figure 16 shows the cost breakthrough, in this case the most expensive components is the MGT due to the higher number of components, in particular the intercooler, which significantly affect plant's cost. Despite its higher power output, the high capital cost results in a higher levelised cost of energy compared to the normal recuperated cycle

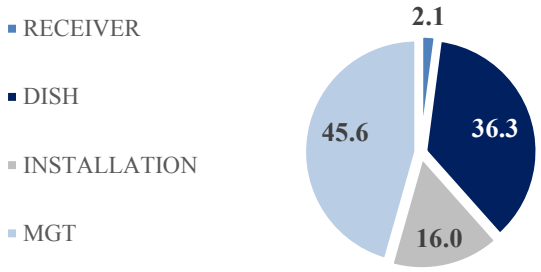

Figure 16. Intercooled and reheated recuperated plant cost breakthrough.

CONCLUSIONS

In this study, a multi-objective optimisation of a hybrid micro turbine-based CSP plant was carried out. The objective of the optimisation was to minimise both LCOE and emissions. A performance evaluation model for each component was presented first, including cost and emissions functions. A sensitivity analysis was then performed in order to select the optimisation variables. This analysis demonstrates that, for this application, the higher the combustor inlet temperature and rotational speed, the lower the levelised cost of energy, with clear benefits also for emissions. The optimisation was performed for two different plant layouts, considering an operational strategy with constant TIT. Results of the optimisation demonstrate that, despite its lower power output, the recuperative Brayton-Joule cycle boost a lower LCOE and lower emissions when compared with an intercooled and reheated recuperative cycle. In the first case, a minimum value for the LCOE of 38.55 €cts/kWh was found. In the second arrangement, the optimisation shows a minimum LCOE around 50.4 €cts/kWh.

This study highlights that, to achieve a lower levelised cost of energy further improvements in the plant components performances are needed. This is especially true for the receiver, the efficiency of which strongly affects the performance of the plant. Another important aspect is the possibility to increase turbine and combustor inlet temperature and a careful selection of the materials could be the key in achieving a competitive cost of energy. Obviously high performance materials results in more expensive components and further investigations to find the correct trade-off are needed.

Abbreviations

CSP = Concentrated Solar Power.
DNI = Direct Normal Irradiation.
MGT= Micro Gas Turbine.
NTU= Number of transfer units.
LCOE= Levelised cost of energy.

NOMENCLATURE

A = Overall heat transfer area [m^2].
C = Cost [€]
C_p = Specific heat (constant pressure) [kJ/ kg K].
E_{NET} = Annual net produced energy [kWh].
f = Friction factor.
f_m = material cost coefficient.
G = Volumetric flow rate [m^3/s].
h = Heat transfer coefficient [W/ m^2K]; enthalpy [J/kg].
J = Colburn Number
k = Thermal Conductivity [W/ m K].
m = expansion polytrophic exponent.
$\dot{m}$ = Mass flow rate [kg/s].
p = pressure [kPa].
P= Power [kW].
Pr = Prandtl Number.
PR = Pressure ratio.
Re = Reynolds Number.
T = Temperature [K].
U =v Overall heat transfer coefficient [W/ m^2K].
V= olume [m^3].

Greek Symbols

δ = thickness [m].
ε = Recuperator effectiveness.
μ= $\dot{m}\sqrt{TIT}\ /p_{t,in}$ corrected mass flow.[$kg\sqrt{K}\ /pa * s$]
η = efficiency.
ρ = Density [kg/ m^3].

Suffix

0 = Total condition.
1 = Recuperator fluid side 1.
2 = Recuperator fluid side 2.
c = Compressor.
cc = Combustion Chamber.
ds = design condition.
i = intercooler.
in = heat exchanger inlet cold side; inlet
p = Polytrophic.
r = recuperator.
rec = Receiver.
ref = reference.
t = Turbine.
TS=Total to Static.
o = off-set fin side 1.
off = off-design condition
out = combustor outlet.
w = wall.

REFERENCES

[1] Botha B. W., Moolman A. (2005). Determining the Impact of the Different Losses on Centrifugal Compressor Design, R & D journal, 21 (3).

[2] Galanti L. and Massardo A. (2011). Micro Gas Turbine Thermodynamic and Economic Analysis up to 500 kWe size. Applied Energy 88 (2011) 4795–4802.

[3] Gallup D.R. (1994). A Solarized Brayton Engine based on turbocharger technology and the DLR receiver. Intersociety Energy Conversion Engineering Conference, (pp. 1719-1729). Monterey.

[4] Ho Sung L. 2011. Thermal Design: Heat Sinks, Thermoelectrics, Heat Pipes, Compact Heat Exchangers, and Solar Cells. John Wiley & Sons.

[5] Iaria D., Al Zaili J. and Sayma A. (2016). Multi-objective optimisation of a centrifugal compressor for a micro gas turbine operated by concentrated solar power. Global Power and Propulsion society forum, Zurich, January 2017, GPPF-2017-33.

[6] Kurzke J. (2012). GasTurb12 user manual.

[7] Lanchi M., Montecchi M., Crescenzi T., Mele D., Miliozzi A., Mazzei D., Misceo M., Falchetta M., Mancini R. (2015). Investigation into the coupling of Micro Gas Turbines with CSP technology: OMSoP project. Energy Procedia 69 (2015) 1317 – 1326.

[8] Lefevbre A. H. (2010). Gas Turbine Combustion: Alternative Fuels and emissions. CRC Press Inc.

[9] Lovegrove K, Stein W. (2012). Concentrating Solar Power Technology. Woodhead Publishing.

[10] Mustafa H., Japikse D., Baines N. C. and M. Zelesky (2003), Axial and Radial Turbines. USA: Concepts NREC.

[11] Qiu K., Yan L., Ni M., Wang C., Xiao G., Luo Z., Cen K. (2015). Simulation and experimental study of an air tube-cavity solar receiver. Energy Conversion and Management 103 (2015) 847–858.

[12] Ragnolo G., Aichmayer L., Wang W., Strand T. and Laumert B. (2014). Technoeconomic design of a micro gas-turbine for a solar dish system. Energy Procedia 69 (2015) 1133 – 1142.

[13] Robertson C.S., Ehede C.L., Stacy L.E.,Abujawdeh S.S., Narayanan R., McCreight L.R., Gatii A. and Rauch H.W. (1980). A conceptual design study of a high temperature solar thermal receiver. NASA technical report, 1980.

[14] Spence S. W. T., Artt D. W. (1997). Experimental performance evaluation of a 99.0 mm radial inflow nozzled turbine with different stator throat areas. Proceedings of the Institution of Mechanical Engineers; 1997; 211, 6.

[15] Yang Y., Li Y., General prediction of the thermal hydraulic performance for plate-fin heat exchanger with offset strip fins (2014), International journal of heat and mass transfer, Volume 78, Pages 860–870.

[16] Wang W., Cai R. and Zhang N., General Characteristics of Single Shaft Microturbine Set at Variable Speed Operation and its Optimization, Applied Thermal Engineering, vol. 24, p. 1851–1863, 2004.

[17] Whitefield and Baines N. C. (1990). Design of Radial Turbomachines. John Wiley & Sons.

[18] Zou C., Zhang Y., Falcoz Q., Neveu P., Zhang C., Shu W. and Huang S. (2017). Design and Optimization of a High- Temperature Cavity Receiver for a Solar Energy Cascade Utilization System. Renewable Energy 103 (2017) 478-489.